Observation of the Identical Rigidity Dependence of He, C, and O Cosmic Rays at High Rigidities by the Alpha Magnetic Spectrometer on the International Space Station

M. Aguilar,[27] L. Ali Cavasonza,[1] B. Alpat,[32] G. Ambrosi,[32] L. Arruda,[25] N. Attig,[22] S. Aupetit,[18] P. Azzarello,[17] A. Bachlechner,[1] F. Barao,[25] A. Barrau,[18] L. Barrin,[16] A. Bartoloni,[37] L. Basara,[35] S. Başeğmez-du Pree,[6] M. Battarbee,[45] R. Battiston,[35,36,a] U. Becker,[10] M. Behlmann,[10] B. Beischer,[1] J. Berdugo,[27] B. Bertucci,[32,33] K. F. Bindel,[23] V. Bindi,[20] W. de Boer,[23] K. Bollweg,[21] V. Bonnivard,[18] B. Borgia,[37,38] M. J. Boschini,[29] M. Bourquin,[17] E. F. Bueno,[39] J. Burger,[10] W. J. Burger,[35] F. Cadoux,[17] X. D. Cai,[10] M. Capell,[10] S. Caroff,[3] J. Casaus,[27] G. Castellini,[15] F. Cervelli,[34] M. J. Chae,[40] Y. H. Chang,[11] A. I. Chen,[10] G. M. Chen,[6] H. S. Chen,[6,7] L. Cheng,[41] H. Y. Chou,[11] E. Choumilov,[10] V. Choutko,[10] C. H. Chung,[1] C. Clark,[21] R. Clavero,[24] G. Coignet,[3] C. Consolandi,[20] A. Contin,[8,9] C. Corti,[20] W. Creus,[44] M. Crispoltoni,[32,33] Z. Cui,[41] K. Dadzie,[10] Y. M. Dai,[5] A. Datta,[20] C. Delgado,[27] S. Della Torre,[29] O. Demakov,[10] M. B. Demirköz,[2] L. Derome,[18] S. Di Falco,[34] F. Dimiccoli,[35,36] C. Díaz,[27] P. von Doetinchem,[20] F. Dong,[31] F. Donnini,[32,33] M. Duranti,[32] D. D'Urso,[32,b] A. Egorov,[10] A. Eline,[10] T. Eronen,[45] J. Feng,[44,10,c] E. Fiandrini,[32,33] P. Fisher,[10] V. Formato,[32] Y. Galaktionov,[10] G. Gallucci,[34] R. J. García-López,[24] C. Gargiulo,[16] H. Gast,[1] I. Gebauer,[23] M. Gervasi,[29,30] A. Ghelfi,[18] F. Giovacchini,[27] D. M. Gómez-Coral,[28] J. Gong,[31] C. Goy,[3] V. Grabski,[28] D. Grandi,[29] M. Graziani,[23] K. H. Guo,[19] S. Haino,[44] K. C. Han,[26] Z. H. He,[19] M. Heil,[10] J. Hoffman,[20] T. H. Hsieh,[10] H. Huang,[44,d] Z. C. Huang,[19] C. Huh,[14] M. Incagli,[34] M. Ionica,[32] W. Y. Jang,[14] Yi Jia,[10] H. Jinchi,[26] S. C. Kang,[14] K. Kanishev,[35,16] B. Khiali,[11] G. N. Kim,[14] K. S. Kim,[14] Th. Kirn,[1] C. Konak,[2] O. Kounina,[10] A. Kounine,[10] V. Koutsenko,[10] A. Kulemzin,[10] G. La Vacca,[29,30] E. Laudi,[16] G. Laurenti,[8] I. Lazzizzera,[35,36] A. Lebedev,[10] H. T. Lee,[43] S. C. Lee,[44] C. Leluc,[17] H. S. Li,[42] J. Q. Li,[31] Q. Li,[31] T. X. Li,[19] Y. Li,[17,c] Z. H. Li,[6] Z. Y. Li,[44,c] S. Lim,[14] C. H. Lin,[44] P. Lipari,[37] T. Lippert,[22] D. Liu,[11] Hu Liu,[27,10,e] V. D. Lordello,[39] S. Q. Lu,[44,c] Y. S. Lu,[6] K. Luebelsmeyer,[1] F. Luo,[41] J. Z. Luo,[31] S. S. Lyu,[19] F. Machate,[1] C. Mañá,[27] J. Marín,[27] T. Martin,[21] G. Martínez,[27] N. Masi,[8] D. Maurin,[18] A. Menchaca-Rocha,[28] Q. Meng,[31] V. M. Mikuni,[39] D. C. Mo,[19] P. Mott,[21] T. Nelson,[20] J. Q. Ni,[19] N. Nikonov,[1] F. Nozzoli,[32,f] A. Oliva,[27] M. Orcinha,[25] F. Palmonari,[8,9] C. Palomares,[27] M. Paniccia,[17] M. Pauluzzi,[32,33] S. Pensotti,[29,30] C. Perrina,[17] H. D. Phan,[10] N. Picot-Clemente,[13] F. Pilo,[34] C. Pizzolotto,[32,g] V. Plyaskin,[10] M. Pohl,[17] V. Poireau,[3] L. Quadrani,[8,9] X. M. Qi,[19] X. Qin,[10] Z. Y. Qu,[44,h] T. Räihä,[1] P. G. Rancoita,[29] D. Rapin,[17] J. S. Ricol,[18] S. Rosier-Lees,[3] A. Rozhkov,[10] D. Rozza,[29,30] R. Sagdeev,[12] S. Schael,[1] S. M. Schmidt,[22] A. Schulz von Dratzig,[1] G. Schwering,[1] E. S. Seo,[13] B. S. Shan,[4] J. Y. Shi,[31] T. Siedenburg,[1] D. Son,[14] J. W. Song,[41] M. Tacconi,[29,30] X. W. Tang,[6] Z. C. Tang,[6] D. Tescaro,[24] Samuel C. C. Ting,[10,16] S. M. Ting,[10] N. Tomassetti,[32,33] J. Torsti,[45] C. Türkoğlu,[2] T. Urban,[21] V. Vagelli,[32,33] E. Valente,[37,38] E. Valtonen,[45] M. Vázquez Acosta,[24] M. Vecchi,[39] M. Velasco,[27] J. P. Vialle,[3] V. Vitale,[35,f] S. Vitillo,[17] L. Q. Wang,[41] N. H. Wang,[41] Q. L. Wang,[5] X. Wang,[10] X. Q. Wang,[6,7] Z. X. Wang,[19] C. C. Wei,[44,i] Z. L. Weng,[10] K. Whitman,[20] H. Wu,[31] X. Wu,[17] R. Q. Xiong,[31] W. Xu,[10] Q. Yan,[10] J. Yang,[40] M. Yang,[6] Y. Yang,[42] H. Yi,[31] Y. J. Yu,[5] Z. Q. Yu,[6] M. Zannoni,[29,30] S. Zeissler,[23] C. Zhang,[6] F. Zhang,[6] J. Zhang,[10,d] J. H. Zhang,[31] S. W. Zhang,[6,7] Z. Zhang,[10] Z. M. Zheng,[4] H. L. Zhuang,[6] V. Zhukov,[1] A. Zichichi,[8,9] N. Zimmermann,[1] and P. Zuccon[10]

(AMS Collaboration)

[1]*I. Physics Institute and JARA-FAME, RWTH Aachen University, D-52056 Aachen, Germany*
[2]*Department of Physics, Middle East Technical University (METU), 06800 Ankara, Turkey*
[3]*Laboratoire d'Annecy-le-Vieux de Physique des Particules (LAPP), CNRS/IN2P3 and Université Savoie Mont Blanc, F-74941 Annecy-le-Vieux, France*
[4]*Beihang University (BUAA), Beijing 100191, China*
[5]*Institute of Electrical Engineering (IEE), Chinese Academy of Sciences, Beijing 100190, China*
[6]*Institute of High Energy Physics (IHEP), Chinese Academy of Sciences, Beijing 100049, China*
[7]*University of Chinese Academy of Sciences (UCAS), Beijing 100049, China*
[8]*INFN Sezione di Bologna, I-40126 Bologna, Italy*
[9]*Università di Bologna, I-40126 Bologna, Italy*
[10]*Massachusetts Institute of Technology (MIT), Cambridge, Massachusetts 02139, USA*
[11]*National Central University (NCU), Chung-Li, Tao Yuan 32054, Taiwan*
[12]*East-West Center for Space Science, University of Maryland, College Park, Maryland 20742, USA*
[13]*IPST, University of Maryland, College Park, Maryland 20742, USA*
[14]*CHEP, Kyungpook National University, 41566 Daegu, Korea*

[15]CNR-IROE, I-50125 Firenze, Italy
[16]European Organization for Nuclear Research (CERN), CH-1211 Geneva 23, Switzerland
[17]DPNC, Université de Genève, CH-1211 Genève 4, Switzerland
[18]Laboratoire de Physique Subatomique et de Cosmologie (LPSC), CNRS/IN2P3 and Université Grenoble-Alpes,
F-38026 Grenoble, France
[19]Sun Yat-Sen University (SYSU), Guangzhou 510275, China
[20]Physics and Astronomy Department, University of Hawaii, Honolulu, Hawaii 96822, USA
[21]National Aeronautics and Space Administration Johnson Space Center (JSC),
Jacobs Engineering, and Business Integra, Houston, Texas 77058, USA
[22]Jülich Supercomputing Centre and JARA-FAME, Research Centre Jülich, D-52425 Jülich, Germany
[23]Institut für Experimentelle Teilchenphysik, Karlsruhe Institute of Technology (KIT), D-76131 Karlsruhe, Germany
[24]Instituto de Astrofísica de Canarias (IAC), E-38205 La Laguna, and Departamento de Astrofísica,
Universidad de La Laguna, E-38206 La Laguna, Tenerife, Spain
[25]Laboratório de Instrumentação e Física Experimental de Partículas (LIP), P-1000 Lisboa, Portugal
[26]National Chung-Shan Institute of Science and Technology (NCSIST), Longtan, Tao Yuan 32546, Taiwan
[27]Centro de Investigaciones Energéticas, Medioambientales y Tecnológicas (CIEMAT), E-28040 Madrid, Spain
[28]Instituto de Física, Universidad Nacional Autónoma de México (UNAM), Mexico, D. F. 01000 Mexico
[29]INFN Sezione di Milano-Bicocca, I-20126 Milano, Italy
[30]Università di Milano-Bicocca, I-20126 Milano, Italy
[31]Southeast University (SEU), Nanjing 210096, China
[32]INFN Sezione di Perugia, I-06100 Perugia, Italy
[33]Università di Perugia, I-06100 Perugia, Italy
[34]INFN Sezione di Pisa, I-56100 Pisa, Italy
[35]INFN TIFPA, I-38123 Povo, Trento, Italy
[36]Università di Trento, I-38123 Povo, Trento, Italy
[37]INFN Sezione di Roma 1, I-00185 Roma, Italy
[38]Università di Roma La Sapienza, I-00185 Roma, Italy
[39]Instituto de Física de São Carlos, Universidade de São Paulo, CP 369, 13560-970 São Carlos, São Paulo, São Paulo, Brazil
[40]Department of Physics, Ewha Womans University, Seoul 120-750, Korea
[41]Shandong University (SDU), Jinan, Shandong 250100, China
[42]National Cheng Kung University, Tainan 70101, Taiwan
[43]Academia Sinica Grid Center (ASGC), Nankang, Taipei 11529, Taiwan
[44]Institute of Physics, Academia Sinica, Nankang, Taipei 11529, Taiwan
[45]Space Research Laboratory, Department of Physics and Astronomy, University of Turku, FI-20014 Turku, Finland

We report the observation of new properties of primary cosmic rays He, C, and O measured in the rigidity (momentum/charge) range 2 GV to 3 TV with 90×10^6 helium, 8.4×10^6 carbon, and 7.0×10^6 oxygen nuclei collected by the Alpha Magnetic Spectrometer (AMS) during the first five years of operation. Above 60 GV, these three spectra have identical rigidity dependence. They all deviate from a single power law above 200 GV and harden in an identical way.

Helium, carbon, and oxygen are among the most abundant nuclei in cosmic rays. They are called primary cosmic rays and are thought to be mainly produced and accelerated in astrophysical sources. Precise knowledge of their spectra in the GV-TV rigidity region provides important insights to the origin, acceleration, and subsequent propagation processes of cosmic rays in the Galaxy [1].

Previously, the precision measurement of the helium flux with the AMS has been reported [2] based on 50×10^6 helium events collected over the first 2.5 years of operations.

Over the last 30 years, there have been many measurements of carbon and oxygen fluxes [3–12]. Typically these measurements have errors larger than 15% at 100 GV.

In this Letter we report the precise measurements of the helium, carbon, and oxygen fluxes in cosmic rays in the rigidity range from 1.9 GV to 3 TV for helium and carbon, and 2.2 GV to 3 TV for oxygen based on data collected by AMS during the first five years (May 19, 2011 to May 26, 2016) of operation aboard the International Space Station (ISS). The total error is ∼3% at 100 GV for both

the carbon and oxygen fluxes and ~1.5% at 100 GV for the helium flux.

Detector.—The layout and description of the Alpha Magnetic Spectrometer (AMS) detector are presented in Ref. [13]. The key elements used in this measurement are the permanent magnet [14], the silicon tracker [15], and the four planes of time of flight (TOF) scintillation counters [16]. Further information on the performance of the TOF is included in the *Detector* section of the Supplemental Material (SM) [17]. The AMS also contains a transition radiation detector (TRD), a ring imaging Čerenkov detector (RICH), an electromagnetic calorimeter (ECAL), and an array of 16 anticoincidence counters.

The tracker has nine layers, the first ($L1$) at the top of the detector, the second ($L2$) above the magnet, six ($L3$ to $L8$) within the bore of the magnet, and the last ($L9$) above the ECAL. $L2$ to $L8$ constitute the inner tracker.

Each layer of the tracker provides an independent measurement of the charge Z with a resolution of $\Delta Z/Z =$ 9% for helium, 5% for carbon, and 4% for oxygen. Overall, the inner tracker has a resolution of $\Delta Z/Z = 3.5\%$ for helium, 2% for carbon, and 1.5% for oxygen.

The spatial resolution in each tracker layer is 6.5 μm in the bending direction for helium, 5.1 μm for carbon, and 6.3 μm for oxygen [18]. Together, the tracker and the magnet measure the rigidity R of charged cosmic rays, with a maximum detectable rigidity (MDR) of 3.2 TV for helium, 3.7 TV for carbon, and 3.4 TV for oxygen over the 3 m lever arm from $L1$ to $L9$.

Helium, carbon, and oxygen nuclei traversing AMS were triggered as described in Ref. [2]. The trigger efficiencies have been measured to be >94% for helium and >97% for carbon and oxygen over the entire rigidity range.

Monte Carlo (MC) simulated events were produced using a dedicated program developed by the collaboration based on the GEANT-4.10.1 package [19]. The program simulates electromagnetic and hadronic interactions of particles in the material of the AMS and generates detector responses. The Glauber-Gribov model [19] tuned to reproduce the AMS helium data, see Fig. SM 1(a) and SM 1(b) in Ref. [2], was used for the description of the nuclei inelastic cross sections.

Event selection.—In the first five years, the AMS has collected 8.5×10^{10} cosmic ray events. The collection time used in this analysis includes only those seconds during which the detector was in normal operating conditions and, in addition, the AMS was pointing within 40° of the local zenith and the ISS was outside of the South Atlantic Anomaly. Because of the geomagnetic field, this collection time increases with rigidity, becoming constant at 1.23×10^8 s above 30 GV.

Helium events were selected as described in Ref. [2]. After selection the event sample contains 90×10^6 helium events with a purity >99.9%.

Carbon and oxygen events are required to be downward going and to have a reconstructed track in the inner tracker which passes through $L1$. In the highest rigidity region, $R \geq 1.13$ TV, the track is also required to pass through $L9$. Track fitting quality criteria such as a $\chi^2/\text{d.o.f.} < 10$ in the bending coordinate are applied, similar to Refs. [2,20,21].

The measured rigidity is required to be greater than a factor of 1.2 times the maximum geomagnetic cutoff within the AMS field of view. The cutoff was calculated by backtracing [22] particles from the top of the AMS out to 50 Earth's radii using the most recent IGRF model [23].

Charge measurements on $L1$, the inner tracker, the upper TOF, the lower TOF, and, for $R > 1.13$ TV, $L9$ are required to be compatible with charge $Z = 6$ for carbon and $Z = 8$ for oxygen, as shown in Fig. 1 of the SM [17] for the inner tracker. This selection yields purities of 99% for carbon and >99.8% for oxygen. The residual backgrounds for carbon and oxygen are discussed in the *Event Selection* section of the SM [17] and in Ref. [24]. After background subtraction we obtain 8.4×10^6 carbon and 7.0×10^6 oxygen nuclei. The overall uncertainty due to background
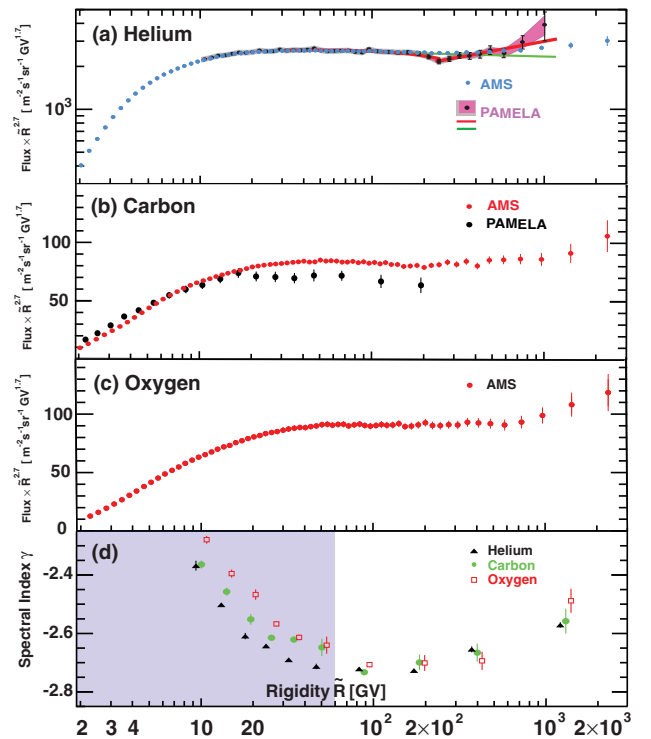
FIG. 1. The AMS (a) helium, (b) carbon, and (c) oxygen fluxes [17] multiplied by $\tilde{R}^{2.7}$ with their total errors as functions of rigidity. Earlier measurements of helium, see Fig. 4 in Ref. [28], and carbon [12] fluxes in rigidity are also shown. (d) The dependence of the helium, carbon, and oxygen spectral indices on rigidity. In (d), for clarity, the horizontal positions of the helium and oxygen data points are displaced with respect to carbon. As seen, above 60 GV (indicated by the unshaded region) the spectral indices are identical.

subtraction is <0.5% for carbon and negligible for oxygen over the entire rigidity range.

Data analysis.—The isotropic flux Φ_i in the ith rigidity bin $(R_i, R_i + \Delta R_i)$ is given by

$$\Phi_i = \frac{N_i}{A_i \epsilon_i T_i \Delta R_i}, \qquad (1)$$

where N_i is the number of events corrected for bin-to-bin migration, A_i is the effective acceptance, ϵ_i is the trigger efficiency, and T_i is the collection time. In this Letter, the helium and carbon fluxes were measured in 68 bins from 1.9 GV to 3.0 TV, and the oxygen flux was measured in 67 bins from 2.2 GV to 3.0 TV with bin widths chosen according to the rigidity resolution. The bin widths are identical for all nuclei.

The bin-to-bin migration of events was corrected using the unfolding procedure described in Ref. [20] independently for the helium, carbon, and oxygen samples. These corrections, $(N_i - \aleph_i)/\aleph_i$ where $\aleph_i$ is the number of observed events in bin i, are +14% at 3 GV, +6% at 5 GV, −4% at 150 GV, and −6% at 3 TV for carbon and very similar for oxygen. For helium, these corrections are very close to those published in Ref. [2].

Extensive studies were made of the systematic errors. These errors include the uncertainties in the background estimations discussed above, the trigger efficiency, the geomagnetic cutoff factor, the acceptance calculation, the rigidity resolution function, and the absolute rigidity scale.

The systematic error on the fluxes associated with the trigger efficiency measurement is <0.7% for these nuclei over the entire rigidity range.

The geomagnetic cutoff factor was varied from 1.0 to 1.4, resulting in a negligible systematic uncertainty (<0.1%) in the rigidity range below 30 GV.

The effective acceptances A_i were calculated using MC simulation and corrected for small differences between the data and simulated events related to (a) event reconstruction and selection, namely in the efficiencies of velocity determination, track finding, charge determination, and tracker quality cuts and (b) the details of inelastic interactions of nuclei in the AMS materials. The total corrections to the acceptance were found to be <2.5% up to 500 GV and <3.5% at 3 TV for helium and carbon, and <3.5% up to 500 GV and <5.0% at 3 TV for oxygen. The systematic errors on the fluxes associated with the reconstruction and selection are <1% over the entire rigidity range for all nuclei.

The material traversed by nuclei between $L1$ and $L9$ is composed primarily of carbon and aluminum. The helium flux systematic errors due to uncertainties in the inelastic cross sections for $He + C$ and $He + Al$ were discussed in detail in Ref. [2]. The systematic error on the carbon and oxygen fluxes due to uncertainties of inelastic cross sections was evaluated in a similar way as discussed in detail in the

Data Analysis section of the SM [17] using data from Ref. [25] and found to be <2.2% for C and <2.7% for O up to 100 GV and 3% for C and 3.5% for O at 3 TV.

The rigidity resolution functions $\Delta(1/R)$ for helium, carbon, and oxygen have a pronounced Gaussian core characterized by widths σ and non-Gaussian tails more than 2.5σ away from the center [2]. The resolution functions have been verified with the procedures described in detail in Ref. [21]. As an example, Fig. 4 of the SM [17] shows that the measured tracker bending coordinate accuracies of 6.5 μm for helium, 5.1 μm for carbon, and 6.3 μm for oxygen are in a good agreement with the simulation. This yields MDRs of 3.2 TV for helium, 3.7 TV for carbon, and 3.4 TV for oxygen with 5% uncertainty. This also provides the uncertainties of 10% on the amplitudes of the non-Gaussian tails. The systematic error on the fluxes due to the rigidity resolution functions was obtained by repeating the unfolding procedure while varying the widths of the Gaussian cores of the resolution functions by 5% and by independently varying the amplitudes of the non-Gaussian tails by 10%. The resulting systematic error on the fluxes is less than 1% below 300 GV and 4% at 3 TV for these nuclei.

There are two contributions to the systematic uncertainty on the rigidity scale [20]. The first is due to residual tracker misalignment. This error was estimated by comparing the E/p ratio for electrons and positrons, where E is the energy measured with the ECAL and p is the momentum measured with the tracker. It was found to be $1/30$ TV^{-1} [26]. The second systematic error on the rigidity scale arises from the magnetic field map measurement and its temperature corrections. The error on the helium, carbon, and oxygen fluxes due to uncertainty on the rigidity scale is <1% up to 300 GV and 6.5% at 3 TV.

Much effort has been spent in understanding the systematic errors [2,20,21]. For this Letter, additional verification was performed. Figure 5 of the SM [17] shows the ratio of two measurements for the (a) carbon and (b) oxygen fluxes from 2.2 GV to 1.13 TV performed using events passing through $L1$ to $L8$, with MDR 1.5 TV for carbon and 1.3 TV for oxygen, and using events passing through $L1$ to $L9$. The good agreement between the measurements verifies the systematic errors on unfolding, due to the difference in the resolution functions, and the systematic errors on acceptance, due to the difference in geometric factor and the amount of material traversed.

Most importantly, several independent analyses were performed on the same data sample by different study groups. The results of those analyses are consistent with this Letter.

Results.—The measured helium, carbon, and oxygen fluxes including statistical and systematic errors are reported in Tables I, II, and III of the SM [17] as functions of the rigidity at the top of the AMS detector.

Figure 1 shows the (a) helium, (b) carbon, and (c) oxygen fluxes as functions of rigidity with their total errors, the

quadratic sum of statistical and systematic errors. In this and the subsequent figures, the points are placed along the abscissa at $\tilde{R}$ calculated for a flux $\propto R^{-2.7}$ [27]. Earlier measurements of the helium [28] and carbon [12] fluxes in rigidity are also shown. The AMS measurement of the helium flux is distinctly different from the results of Ref. [28] which shows a sharp spectrum shape change. The AMS measurement of the carbon flux is also distinctly different from the results of Ref. [12], which are 20–25% lower above 20 GV.

To examine the rigidity dependence of the fluxes, the variation of the flux spectral indices with rigidity was obtained in a model independent way. The flux spectral indices were calculated from

$$\gamma = d[\log(\Phi)]/d[\log(R)] \qquad (2)$$

over nonoverlapping rigidity intervals above 8.48 GV, with a variable width to have sufficient sensitivity to determine γ. The results are presented in Fig. 1(d). As seen, the magnitude and the rigidity dependence of the helium, carbon, and oxygen spectral indices are very similar. In particular, all spectral indices are identical within the measurement errors above 60 GV and all spectral indices harden with rigidity above ~200 GV.

Figure 2 shows the AMS (a) helium, (b) carbon, and (c) oxygen fluxes as a function of kinetic energy per nucleon E_K together with the results of previous experiments. At high energies, the AMS measurement of the helium flux is distinctly different from the previous experiments. The AMS measurements of the carbon and oxygen fluxes at high energies are also very different from previous measurements, being about 20–40% higher above 10 GeV/n.

To examine the difference between the rigidity dependence of the helium, carbon, and oxygen fluxes in detail, first, the ratio of the helium flux to the oxygen flux, or He/O ratio, was computed using the data in Tables I and III of the SM [17], and it was reported in Table IV of the SM [17], with its statistical and systematic errors.

Figure 3(a) shows the He/O ratio with total errors, the quadratic sum of statistical and systematic errors, together with the cosmic ray propagation model GALPROP [31] prediction based on data available before the AMS. As seen in Fig. 3(a), above 60 GV the He/O ratio measured by the AMS is well fit by a constant value of 27.9 ± 0.6 with a $\chi^2/\mathrm{d.o.f.} = 16/27$. This is in disagreement with the GALPROP model which predicts a He/O ratio decreasing with rigidity. Figure 6 of the SM [17] shows the AMS He/O ratio as a function of kinetic energy per nucleon E_K together with the results of a previous experiment [6].

Similarly, the ratio of the carbon flux to the oxygen flux, or the C/O ratio, was computed using the data in Tables II and III of the SM [17] and reported in Table V of SM [17], with its statistical and systematic errors. Figure 3(b) shows the C/O ratio with total errors together with the GALPROP
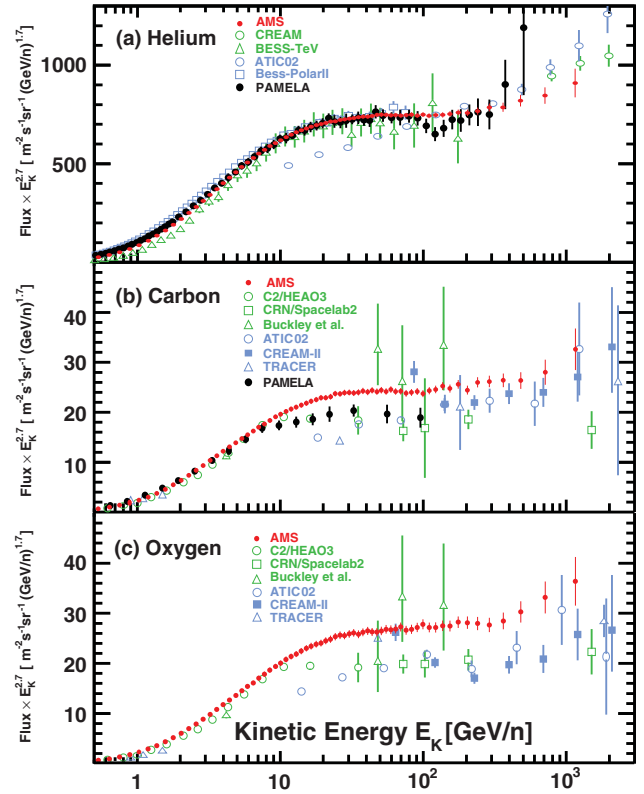
FIG. 2. The AMS (a) helium, (b) carbon, and (c) oxygen fluxes as functions of kinetic energy per nucleon E_K multiplied by $E_K^{2.7}$ together with previous measurements [4–12,28,29]. For the AMS measurement $E_K = (\sqrt{Z^2\tilde{R}^2 + M^2} - M)/A$ where Z, M, and A are the ^{4}He, ^{12}C, or ^{16}O charge, mass, and atomic mass numbers, respectively. Data from other experiments were extracted using Ref. [30].

model prediction based on data available before the AMS. As seen in Fig. 3(b), above 60 GV, the C/O ratio measured by the AMS is well fit by a constant value of 0.91 ± 0.02 with a $\chi^2/\mathrm{d.o.f.} = 25/27$. This is again in disagreement with the GALPROP model which predicts a C/O ratio decreasing with rigidity. Figure 7 of the SM [17] shows the AMS C/O ratio as a function of kinetic energy per nucleon E_K together with the results of previous experiments [4,5,7–11]. As seen, the C/O ratio measured by the AMS is within 10% of unity.

It is important to note that, whereas protons, helium, carbon, and oxygen are all considered primary cosmic rays, the independence of the measured C/O and He/O flux ratios with rigidity is completely different from the proton to helium flux ratio rigidity dependence, see Fig. 2(b) of Ref. [2]. None of these unexpected results, including the p/He flux ratio rigidity dependence [24,32], can be explained by the current understanding of cosmic rays.

In conclusion, we have presented precise, high statistics measurements of the helium, carbon, and oxygen fluxes from 2 GV to 3 TV, with detailed studies of the systematic
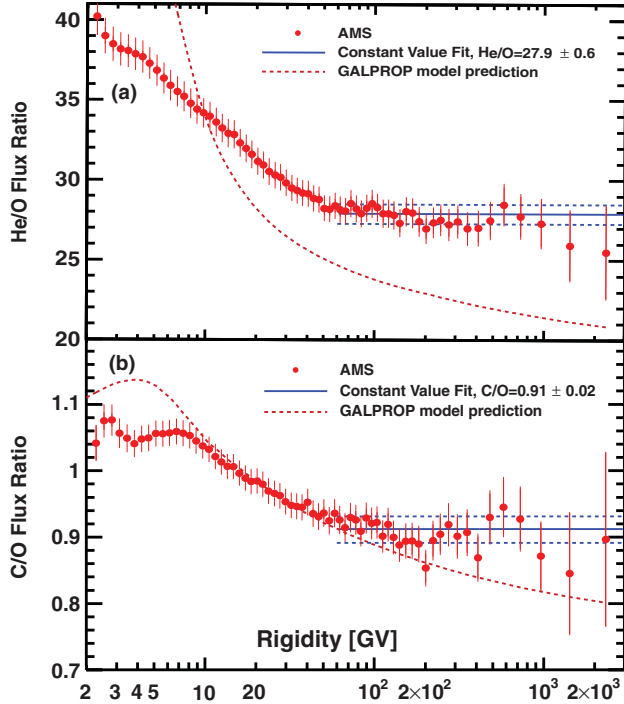
FIG. 3.   The (a) He/O and (b) C/O ratios as functions of rigidity compared with the GALPROP model predictions [31], dashed red curves. The solid blue lines indicate the fits of constant values to the ratios with the dashed blue lines their total errors (1σ). As seen, above 60 GV both the He/O and C/O ratios are well described by constant values of 27.9 ± 0.6 and 0.91 ± 0.02 with $\chi^2/\text{d.o.f.} = 16/27$ and $\chi^2/\text{d.o.f.} = 25/27$, respectively.

errors. These measurements show that the fluxes deviate from a single power law. Their spectral indices all progressively harden above 200 GV. Surprisingly, above 60 GV, the three fluxes have identical rigidity dependence, as illustrated in Fig. 4. Above 60 GV, the helium to oxygen
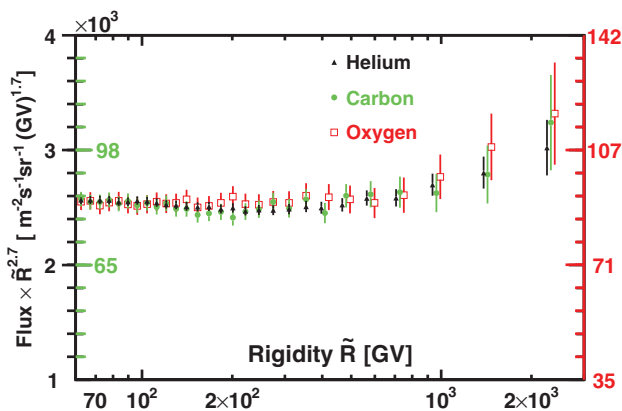
FIG. 4.   The rigidity dependence of the helium (left black axis), carbon (left green axis), and oxygen (right red axis) fluxes. For clarity, horizontal positions of the helium and oxygen data points above 400 GV are displaced with respect to the carbon. As seen, above 60 GV the three fluxes have identical rigidity dependence.

flux ratio is constant at 27.9 ± 0.6 and the carbon to oxygen flux ratio is constant at 0.91 ± 0.02.

---

[a]Also at ASI, I-00133 Roma, Italy.

[b]Also at ASI Space Science Data Center (SSDC), I-00133 Roma, Italy; Present address: University of Sassari, I–07100 Sassari, Italy.

[c]Also at Sun Yat-Sen University (SYSU), Guangzhou, 510275, China.

[d]Also at Wuhan University, Wuhan, 430072, China.

[e]Also at Huazhong University of Science and Technology (HUST), Wuhan, 430074, China.

[f]Also at ASI Space Science Data Center (SSDC), I-00133 Roma, Italy.

[g]Also at ASI Space Science Data Center (SSDC), I-00133 Roma, Italy; Present address: INFN Sezione di Trieste, I–34149, Trieste, Italy.

[h]Also at Nankai University, Tianjin 300071, China.

[i]Also at Institute of Theoretical Physics, Chinese Academy of Sciences, Beijing, 100190, China.

[1] I. A. Grenier, J. H. Black, and A. W. Strong, Annu. Rev. Astron. Astrophys. **53**, 199 (2015); P. Blasi, Astron. Astrophys. Rev. **21**, 70 (2013); A. W. Strong, I. V. Moskalenko, and V. S. Ptuskin, Annu. Rev. Nucl. Part. Sci. **57**, 285 (2007); A. Castellina and F. Donato, Astropart. Phys. **24**, 146 (2005).

[2] M. Aguilar et al., Phys. Rev. Lett. **115**, 211101 (2015).

[3] R. Dwyer and P. Meyer, Astrophys. J. **322**, 981 (1987); M. Simon, H. Spielgelhauer, W. K. H. Schmidt, F. Siohan, J. F. Ormes, V. K. Balasubrahmanyan, and J. F. Arens, Astrophys. J. **239**, 712 (1980); C. D. Orth, A. Buffington, G. F. Smoot, and T. S. Mast, Astrophys. J. **226**, 1147 (1978).

[4] J. J. Engelmann, P. Ferrando, A. Soutoul, P. Goret, and E. Juliusson, Astron. Astrophys. **233**, 96 (1990).

[5] S. P. Swordy, D. Müller, P. Meyer, J. L'Heureux, and J. M. Grunsfeld, Astrophys. J. **349**, 625 (1990).

[6] J. Buckley, J. Dwyer, D. Müller, S. Swordy, and K. K. Tang, Astrophys. J. **429**, 736 (1994).

[7] A. D. Panov et al., Bull. Acad. Sci. USSR, Phys. Ser. **73**, 564 (2009).

[8] H. S. Ahn et al., Astrophys. J. **715**, 1400 (2010); Astrophys. J. **714**, L89 (2010); Astrophys. J. **707**, 593 (2009).

[9] F. Gahbauer, G. Hermann, J. R. Hörandel, D. Müller, and A. A. Radu, Astrophys. J. **607**, 333 (2004).

[10] M. Ave, P. J. Boyle, F. Gahbauer, C. Höppner, J. R. Hörandel, M. Ichimura, D. Müller, and A. Romero-Wolf, Astrophys. J. **678**, 262 (2008).

[11] A. Obermeier, M. Ave, P. Boyle, Ch. Höppner, J. Hörandel, and D. Müller, Astrophys. J. **742**, 14 (2011).

[12] O. Adriani et al., Astrophys. J. **791**, 93 (2014).

[13] A. Kounine, Int. J. Mod. Phys. E **21**, 1230005 (2012); S. Rosier-Lees, in Proceedings of Astroparticle Physics TEVPA/IDM, Amsterdam, 2014 (unpublished); S. Ting, Nucl. Phys. B, Proc. Suppl. **243–244**, 12 (2013); S.-C. Lee, in Proceedings of the 20th International Conference on Supersymmetry and Unification of Fundamental Interactions (SUSY 2012), Beijing, 2012 (unpublished); M. Aguilar, in Proceedings of the XL International Meeting on Fundamental Physics, Centro de Ciencias de Benasque Pedro Pascual, 2012 (unpublished); S. Schael, in Proceedings of the 10th Symposium on Sources and Detection of Dark Matter and Dark Energy in the Universe, Los Angeles, 2012 (unpublished); B. Bertucci, Proc. Sci., EPS-HEP2011 (2011) 67; M. Incagli, AIP Conf. Proc. **1223**, 43 (2010); R. Battiston, Nucl. Instrum. Methods Phys. Res., Sect. A **588**, 227 (2008).

[14] K. Lübelsmeyer et al., Nucl. Instrum. Methods Phys. Res., Sect. A **654**, 639 (2011).

[15] B. Alpat et al., Nucl. Instrum. Methods Phys. Res., Sect. A **613**, 207 (2010).

[16] V. Bindi et al., Nucl. Instrum. Methods Phys. Res., Sect. A **743**, 22 (2014).

[17] See Supplemental Material at http://link.aps.org/supplemental/10.1103/PhysRevLett.119.251101 for details of the AMS detector and the event selection; for the tabulated helium, carbon, and oxygen fluxes, the carbon to oxygen flux ratio, and the helium to oxygen flux ratio, all as functions of rigidity; and also for several figures regarding charge resolution and selection, survival probabilities, tracker residuals, detailed systematic studies, and the C and O fluxes as a function of kinetic energy per nucleon.

[18] G. Ambrosi, V. Choutko, C. Delgado, A. Oliva, Q. Yan, and Y. Li, Nucl. Instrum. Methods Phys. Res., Sect. A **869**, 29 (2017). With large samples of nuclei data, we are able to accurately account for nonlinear saturation effects in the tracker electronics and this has improved the AMS tracker coordinate resolution for nuclei.

[19] J. Allison et al., Nucl. Instrum. Methods Phys. Res., Sect. A **835**, 186 (2016); S. Agostinelli et al., Nucl. Instrum. Methods Phys. Res., Sect. A **506**, 250 (2003).

[20] M. Aguilar et al., Phys. Rev. Lett. **114**, 171103 (2015).

[21] M. Aguilar et al., Phys. Rev. Lett. **117**, 231102 (2016).

[22] J. Alcaraz et al., Phys. Lett. B **484**, 10 (2000).

[23] C. C. Finlay et al., Geophys. J. Int. **183**, 1216 (2010); E. Thébault et al., Earth, Planets Space **67**, 79 (2015).

[24] AMS Collaboration, Measurement of the Flux of Light Nuclei Cosmic Rays with the Alpha Magnetic Spectrometer on the International Space Station (to be published).

[25] M. Takechi et al., Phys. Rev. C **79**, 061601 (2009); T. Zheng et al., Nucl. Phys. **A709**, 103 (2002); H. Y. Zhang et al., Nucl. Phys. **A707**, 303 (2002); A. Ozawa et al., Nucl. Phys. **A691**, 599 (2001); D. Q. Fang et al., Phys. Rev. C **61**, 064311 (2000); S. Kox et al., Phys. Rev. C **35**, 1678 (1987); S. Kox, A. Gamp, R. Cherkaoui, A. J. Cole, N. Longequeue, J. Menet, C. Perrin, and J. B. Viano, Nucl. Phys. **A420**, 162 (1984); V. D. Aksinenko et al., Nucl. Phys. **A348**, 518 (1980); J. Jaros et al., Phys. Rev. C **18**, 2273 (1978).

[26] J. Berdugo, V. Choutko, C. Delgado, and Q. Yan, Nucl. Instrum. Methods Phys. Res., Sect. A **869**, 10 (2017). With five years of data we are able to improve the estimation of residual time dependent tracker misalignment and the tracker rigidity scale estimation. The details of these improvements will be published in the forthcoming review article [25]. The conclusions reached in Ref. [2] remain unchanged.

[27] G. D. Lafferty and T. R. Wyatt, Nucl. Instrum. Methods Phys. Res., Sect. A **355**, 541 (1995). We have used Eq. (6) with $\tilde{R} \equiv x_{lw}$.

[28] O. Adriani *et al.*, Science **332**, 69 (2011).

[29] For the ATIC experiment see A. D. Panov *et al.*, Bull. Acad. Sci. USSR, Phys. Ser. **73**, 564 (2009); extracted from D. Maurin, F. Melot, and R. Taillet, Astron. Astrophys. **569**, A32 (2014); for the BESS experiment see K. Abe *et al.*, Astrophys. J. **822**, 65 (2016); Y. Shikaze *et al.*, Astropart. Phys. **28**, 154 (2007); S. Haino *et al.*, Phys. Lett. B **594**, 35 (2004); T. Sanuki *et al.*, Astrophys. J. **545**, 1135 (2000); for the CREAM experiment see Y. S. Yoon *et al.*, Astrophys. J. **728**, 122 (2011); **765**, 91 (2013).

[30] D. Maurin, F. Melot, and R. Taillet, Astron. Astrophys. **569**, A32 (2014).

[31] We used GALPROP WEBRUN; A. E. Vladimirov, S. W. Digela, G. Jóhannesson, P. F. Michelson, I. V. Moskalenko, P. L. Nolan, E. Orlando, T. A. Porter, and A. W. Strong, Comput. Phys. Commun. **182**, 1156 (2011); with parametrization from R. Trotta, G. Jóhannesson, I. V. Moskalenko, T. A. Porter, R. Ruiz de Austri, and A. W. Strong, Astrophys. J. **729**, 106 (2011).

[32] S. Ting, *Proc. Sci.*, ICRC2015 (2015) 036.